Atmospheric
Chemistry
and Physics
Discussions

Simulations of black carbon (BC) aerosol impact over Hindu-Kush Himalayan sites: validation, sources, and implications on glacier runoff

Sauvik Santra[1], Shubha Verma[1], Koji Fujita[2], Indrajit Chakraborty[1], Olivier Boucher[3], Toshihiko Takemura[4], John F. Burkhart[5], Felix Matt[5], and Mukesh Sharma[6]

[1]Department of Civil Engineering, Indian Institute of Technology Kharagpur, India
[2]Graduate School of Environmental Studies, Nagoya University, Nagoya, Japan
[3]Institut Pierre-Simon Laplace, Centre National de la Recherche Scientifique / Sorbonne Université, 75252 Paris Cedex 05, France
[4]Research Institute for Applied Mechanics, Kyushu University, Fukuoka, Japan
[5]Department of Geosciences, University of Oslo, Norway
[6]Department of Civil Engineering, Indian Institute of Technology Kanpur, India

Correspondence: Shubha Verma (shubha@iitkgp.ac.in)

Abstract. We estimated the black carbon (BC) concentration over the Hindu Kush Himalayan region (HKH), its impact on snow-albedo reduction and sensitivity on annual glacier runoff over the identified glaciers. These estimates were based on free-running aerosol simulations ($freesimu$) and constrained aerosol simulations ($constrsimu$) from an atmospheric general circulation model, combined with numerical simulations of glacial mass balance model. BC concentration estimated from $freesimu$ performed better over higher altitude (HA) HKH stations than that over lower altitude (LA) stations. The estimates from $constrsimu$ mirrored well the measurements when implemented for LA stations. Estimates of the spatial distribution of BC concentration in the snowpack (BC_c) over the HKH region led to identifying a hot-spot zone located around Manora peak. Among glaciers over this zone, BC_c (>60 μg kg^{-1}) and BC-induced snow-albedo reduction ($\approx$5%) were estimated explicitly being high during the pre-monsoon for Pindari, Poting, Chorabari, and Gangotri glaciers (which are major sources of fresh water for the Indian sub-continent). The rate of increase of BC_c in recent years (i.e. over the period 1961–2010) was, however, estimated being the highest for the Zemmu glacier. Sensitivity analysis with glacial mass balance model indicated the increase in annual runoff from debris-free glacier area due to BC-induced snow albedo reduction (SAR) corresponding to BC_c estimated for the HKH glaciers was 4% – 18%, with the highest being for the Milam and Pindari glacier. The rate of increase in annual glacier runoff per unit BC-induced percentage SAR was specifically high for Milam, Pindari, and Shunkalpa glacier. The source-specific contribution to atmospheric BC aerosols by emission sources led to identifying the potential emission source being primarily from the biofuel combustion in the Indo-Gangetic plain south to 30°N, but also from open burning in a more remote region north to 30°N.

1 Introduction

Aerosols are particles in the atmosphere known to impact Earth's climate directly as well as indirectly (Foster, 2007). Aerosols tend to scatter or absorb insolation and thus affect the radiation budget likewise Ramanathan et al. (2001a, b). Among aerosol constituents, black carbon (BC) is a major absorbing aerosol constituent produced from incomplete combustion of biomass,

5 biofuel, and fossil fuel (Bond et al., 2013). Black carbon impacts the climate through a direct effect by absorbing sunlight (Ramanathan and Carmichael, 2008) and an indirect effect through cloud alterations in precipitation efficiency (Lohmann and Feichter, 2005). Another impact due to absorbing aerosols such as BC exists on the cryosphere by altering the ablation rate of ice and snow (Flanner et al., 2007; Painter et al., 2007). Deposited black carbon over snow enhances absorption of solar radiation, darkens the upper mixing layers of the snowpack thereby reducing the snow albedo (Warren and Wiscombe, 1980) and leading

10 to accelerated melting of snow (Jacobson, 2004; Flanner et al., 2007). The Himalayan region has been exposed to particulate pollution and deposition of BC as reported in observational studies at high altitude Himalayan stations (Bonasoni et al., 2012, 2010a, b; Marinoni et al., 2010; Nair et al., 2013; Jacobi et al., 2014). Based on the atmospheric BC measurements at stations (e.g. NCOP, Hanle) over the Hindukush-Himalayan (HKH) region, radiative forcing due to BC and the BC-induced snow albedo reduction (SAR) for estimated BC concentration in snow over the stations was reported in recent studies (Nair et al.,

15 2013; Yasunari et al., 2010). Additionally, the premature ablation of snowpack over the Himalayan region (at Khumbu valley, Nepal), which brought forward the melting of snowpack by 17 to 27 days has also been inferred due to BC-induced snow-albedo reduction (SAR) based on snowpack modelling (Jacobi et al., 2014). Further, the impact of BC aerosols on the snowpack, surface radiation, and temperature changes over the HKH region based on simulations in global climate models suggest a considerable impact of anthropogenic forcing over the HKH region as compared to that over the Tibetan Plateau.

20 However, the ability of coarse-gridded models to simulate adequately the snow depth and thereby the BC concentration in snow and atmospheric BC radiative forcing is limited (Menon et al., 2010; Ménégoz et al., 2014).

The influence of the albedo change on the glacial mass balance due to an excess and preponed snow melting and thereby the glacier runoff is expected to impact the downstream hydrology (Fujita, 2007; Matt et al., 2018; Sakai and Fujita, 2017). This impact is specifically of concern for the HKH region as the Himalayan glaciers are the source of major rivers in South

25 Asia namely Ganges, Indus, Yamuna, and Brahmaputra (also known as Tsangpo). The inaccessible terrain and severe weather conditions in the higher Himalayan region hinder the measurement of atmospheric BC concentration and BC concentration in snow (Ming et al., 2009) at regular spatial as well as temporal intervals. The measured data may thus serve as a location and time specific primary data and not a representative sample of the regional distribution. The simulated BC concentration, using atmospheric chemical transport models (CTMs), which is validated by measurements, can be utilized to predict the spatial

30 mapping of BC distribution over the HKH region. In order to spatially map as adequately as possible the estimates of atmospheric BC concentration and BC concentration in snow including the corresponding SAR over the HKH region, an integrated approach merging the relevant information from observations with a relatively consistent atmospheric chemical transport model estimates is applied in the present study.

In the present study, we evaluate BC concentration estimated from the free running ($freesimu$) aerosol simulations us-

Atmospheric
Chemistry
and Physics
Discussions

ing Laboratoire de Météorologie Dynamique atmospheric General Circulation Model (LMDZT-GCM) and Spectral Radiation Transport Model for Aerosol Species (SPRINTARS) over the HKH region. This evaluation includes comparison of simulated BC concentration with available observations (Nair et al., 2013; Marinoni et al., 2010; Babu et al., 2011) for winter (monthly average of December, January, and February) and pre-monsoon (monthly average of March, April, and May) season, at lo-
5   cations, classified as low-altitude (LA) stations (e.g. Nainital,Kullu, and Dehradun, refer to Figure:1(a)), which are in close proximity to emission sources; and high-altitude (HA) stations (e.g. Hanle, NCO-P, and Satopanth, Figure:1(b)), which are relatively remotely located and mostly influenced by transport of aerosols. Constrained aerosol simulation ($constrsimu$) is also formulated (discussed in Section 2.2) and estimates are evaluated over the LA stations. Details of the simulation used can be found in Table 2. Impact of BC concentration in the snow (BC_c) on SAR is estimated (Section 2.3); and numerical
10   simulations of annual glacier runoff height and snow-albedo are carried out using glacial mass balance model (Section 2.4) to evaluate the impact of BC-induced SAR on increase in annual snowmelt runoff from glaciers. In order to examine the source

Table 1. Description of glaciers considered in this study

Glacier Name (abbreviation)	Lat. ($°N$)	Lon. ($°E$)	Area (km^2)	Elevation (m a.s.l.)	RDCA* (%)	Recession Rate (m y^{-1})	Reference
Bara Shigri (BS)	32.166	77.695	112.4	3931-6438	17.8	30.0	Sangewar and Kulkarni (2011)
Chorabari (CB)	30.786	79.046	4.6	3926-6717	28.1	6.8	Mehta et al. (2014)
Gangotri (GG)	30.800	79.149	136.9	3995-7062	25.9	34.0	Naithani et al. (2001)
Milam (ML)	30.520	80.050	59.2	3552-6989	32.5	25.5	Raj (2011)
Pindari (PD)	30.301	80.007	11.4	3669-6568	7.4	23.4	Vohra (1981)
Poting (PT)	30.235	80.133	4.5	3665-5639	15.0	5.1	Vohra (1981)
Shunkalpa (SK)	30.378	80.320	34.3	3952-6527	24.1	6.8	Vohra (1981)
Sonapani (SP)	32.421	77.355	6.7	3805-5562	0.0	15.9	Vohra (1981)
Zemmu (ZM)	27.743	88.238	68.6	4178-7402	35.6	19.8	Vohra et al. (1993)

[*]RDCA = Ratio of debris-covered area

of BC aerosols over the HKH region due to emissions from combustion sectors and that from nearby or remote region, source- and region-tagged BC simulation in LMDZT-GCM (Verma et al., 2011) is also evaluated.

Hence, the specific objectives of this study includes evaluation of (1) atmospheric BC concentration estimated from $freesimu$
15   and $constrsimu$ over the HKH region, (2) spatial distribution of BC_c and identification of hot-spot zone and glaciers located in this zone, (3) impact of BC_c on SAR over the glaciers and its potential to increase the annual glacier runoff through numerical simulations with a glacial mass balance model, and (4) source of origin of BC aerosols over the HKH region. The hypsometry of nine glaciers taken under study (refer to Table 1 and Section 2.4) is shown in Figure 1(c). The selected glaciers are widely distributed over the HKH region and located near the zone of high BC_c values (discussed in Section 3.2). The out-
20   line of glaciers are based on Glacier Area Mapping for Discharge from the Asian Mountains (GAMDAM) Glacier Inventory (Nuimura et al., 2015).
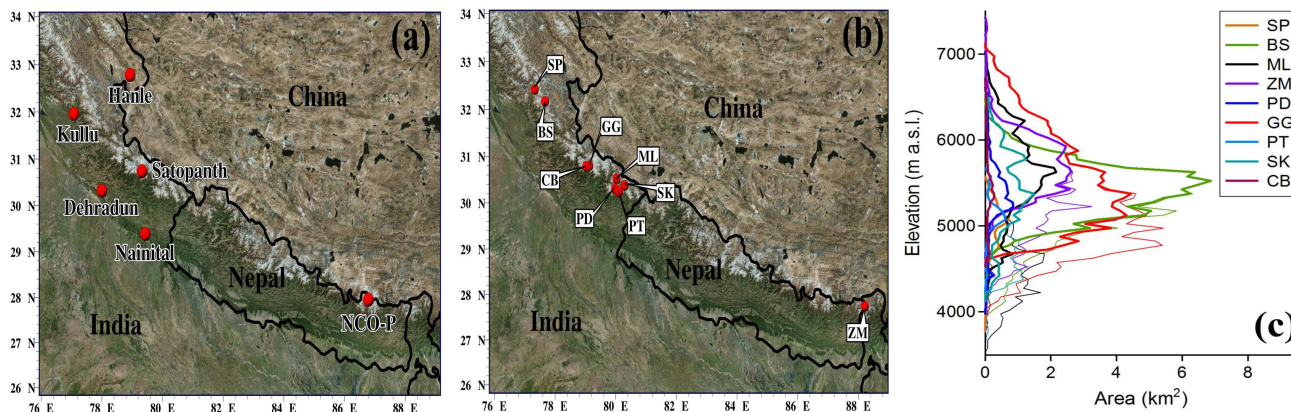
Figure 1. Map of the study domain showing (a) six stations of available measurements and (b) simulated glaciers (c) Hypsometry of nine glaciers. Outline of glaciers are based on GAMDAM Glacier Inventory (Nuimura et al., 2015). Thick and thin lines denote debris-free and debris-covered areas respectively. The debris-covered area was excluded from the calculation. Glacier abbreviations and details are listed in Table:1.

2 Methodology

2.1 Free running BC simulations in GCM

We evaluate BC surface concentration estimated from three $freesimu$ performed with the general circulation model of Laboratoire de Météorologie Dynamique (LMD-ZT GCM) (Hourdin and Armengaud, 1999; Li, 1999; Hourdin et al., 2006) and Spec-

5 tral Radiation Transport Model for Aerosol Species (SPRINTARS) (Takemura, 2012). The two $freesimu$ with the LMD-ZT GCM comprises of (i) LMD-ZT GCM - with India emissions (GCM-indemiss), (ii) LMD-ZT GCM coupled to the Interactions between Aerosols and Chemistry (INCA) model (LMDORINCA)– with global emissions, or namely GCM-INCA. Aerosol simulations in GCM are also referred as free running aerosol simulations ($freesimu$) since simulated aerosol fields are not constrained by observations, unlike constrained simulations (described in Section 2.2). We provide only a very brief description

10 of these models here and detailed information could be obtained from references provided for models. Specific description of aerosol treatment and atmospheric transport for GCM-indemiss (GCM with India emissions) is given by Boucher and Pham (2002); Reddy et al. (2004); Verma et al. (2008), for LMDORINCA by Schulz et al. (2006), and for SPRINTARS by Takemura (2012). GCM-indemiss uses BC emissions over India from Reddy and Venkataraman (2002a, b), over Asia from Streets et al. (2003a), and global emissions of BC are from Cooke et al. (1999); Cooke and Wilson (1996). BC simulation with GCM-

15 indemiss is carried out with a zoom factor of four and three applied in longitude and latitude respectively, having the zoom centralized at 75°E and 15°N, and extending from 50°E to 100°E in longitude and from 5°S to 35°N in latitude; leading to a resolution of 1° in longitude and 0.8° in latitude over the zoomed region. GCM-INCA global emission inventory for BC is from Generoso et al. (2003) and Bond et al. (2004). BC simulation with GCM-INCA is done in non-zoom mode at a horizontal resolution of 3.75° in longitude and 2.5° in latitude. In both GCM model variants 19 vertical layers with a hybrid sigma-pressure

Atmospheric
Chemistry
and Physics
Discussions

coordinate are used, having five layers below 600 hPa and nine layers above 250 hPa. Model meteorological fields are nudged to 6-hourly data from European Centre for Medium-Range Weather Forecast (ECMWF) meteorological analysis data with a relaxation time of 0.1 day for the year of 2001 in GCM-indemiss, for 2006 in GCM-INCA. In order to examine sources of BC aerosol over the HKH region due to emissions from near-by and far-off regions and that from various source sectors (e.g.,

5   residential biofuel use, open burning of biomass, and fossil fuel combustion), region- and source-tagged simulations carried out in GCM-indemiss (Verma et al., 2011, 2008) are evaluated. These simulations were carried out for each of the classified geographical regions (region-tagged simulation), including the Indo-Gangetic plain (IGP), central India (CNI), south India (SI), northwest India (NWI), southeast Asia (SEA), east Asia (EA), Africa/west Asia (AFWA), and rest of the world (ROW) with aerosol emissions outside the region of interest being switched-off.

10   In SPRINTARS, global emission for BC is adopted from the standard inventories for the Coupled Model Inter-comparison Project Phase 5 (CMIP5) (Lamarque et al., 2010; Moss et al., 2010). BC simulation with SPRINTARS is done at a horizontal resolution of approximately $2.8° \times 2.8°$ with 20 vertical layers based on sigma-pressure levels (Takemura, 2012). These simulations are available for a long term period from 1851 to 2010. GCM-indemiss simulation for the year 2001 is compared with SPRINTARS output for 2001 (referred to as SP1). Long-term BC simulation output from SPRINTARS is used to compare

15   model values (referred to as SP2) with observations corresponding to the year of observation. Also, these simulations are used to predict the annual rate of increase in BC concentration over the HKH glaciers as presented in Section 3. The one-sigma uncertainty in mean model simulated atmospheric BC burden based on evaluation in sixteen global aerosol models has been estimated as 42% (Textor et al., 2006).

Table 2. Details of BC simulation used in this study

Aerosol Simulations in GCM (For LA, HA & Glaciers)			
Experiment	Emissions	Resolution (mode)	Simulation year
GCM-indemiss	India[a], Asia[b], Global[c]	$1° \times 0.8° \times 19$ (zoom)	2001
GCM-INCA	Global[d]	$3.75° \times 2.5° \times 19$ (non-zoom)	2006
SPRINTARS	Global[e]	$2.8° \times 2.8° \times 20$	multi-yr. period
Constrained Aerosol Simulations (For LA)			
Experiment, estimated value[f]	Observational data used	Station Name	Year
$Ratio-approach, SC_{bc}^{cr}(i,j,t)$	R_{bc}, ground-truth τ_{500}	Kullu, DDN, NTL	year of measurement[h]
$Profile-approach, SC_{bc}^{cp}(i,j,t)$	CALIPSO profile (σ) [g]	Kullu, DDN, NTL	2008-09

[a] Reddy and Venkataraman (2002a, b); [b] Streets et al. (2003a); [c] Olivier and Berdowski (2001); Cooke et al. (2002); Cooke and Wilson (1996); [d] Bond et al. (2004); Generoso et al. (2003); Olivier and Berdowski (2001); [e] Takemura et al. (2000, 2009); Guenther and et al. (1995); Spiro et al. (1992); [f] Estimated value of aerosol species concentration from constrained simulation compared with observation; [g] Profile of σ to τ at 532 nm from CALIPSO; [h] Observed ground-truth τ_{500} from available studies NTL 2005-12, Kullu 2009-12 and DDN 2007-10;

2.2   Constrained BC simulation

20   The constrained simulation ($constrsimu$) approach takes into account the influence of a possible discrepancy in base emissions, the localized effect of high emission flux (from the plains near LA), and the combined effect of inter-annual variability

Atmospheric
Chemistry
and Physics
Discussions

in meteorological effects (Kumar et al., 2018). This is used to establish an alternate approach for estimating the atmospheric BC concentration by surpassing the error induced specifically due to emissions in source regions which prevail in case of the free running aerosol simulations. In constrained simulations, GCM-indemiss AOD is constrained by the observed AOD. An inversion algorithm is formulated to obtain the surface concentration of BC from constrained AOD of aerosol constituents. It may be notable that constrained simulations are considered only for the LA stations. The HA stations which are far away from the source of emissions, the impact of regional emission bias is postulated to be minor and aerosol pollutants are primarily governed by the atmospheric transport processes (simulated atmospheric residence time) from the surrounding regions. Our postulate is supported by the fact that BC from $freesimu$ of GCM-indemiss that are underestimated by a large factor at LA stations (refer Section 3.1 and Table:4), match consistently well with available observations at HA stations (refer to section:3.1 and figure:2). Hence, in the present study, simulated BC from GCM-indemiss is considered a suitable choice (based on analysis of performance of model with measurements, discussed in Section 3.1) for evaluation of BC-induced SAR and its impact on annual snowmelt runoff from the glaciers under study.

The two constrained simulations formulated using the ratio approach (RA) and profile approach (PA) are compared with measurements. On a fundamental basis the two simulations namely, RA and PA, use BC-AOD (τ_{bc}^m) and total AOD (τ^m) from the $freesimu$ of GCM-indemiss to obtain the ratio R_{bc} as follows:

$$R_{bc}(i,j,\overline{t}) = \frac{\tau_{bc}^m(i,j,\overline{t})}{\sum \tau^m(i,j,\overline{t})} \qquad (1)$$

where $\overline{t}$ specifies the seasonal mean for winter and pre-monsoon. The i and j corresponds to the grid positions on the spatial map with the resolution of 1° x 0.8° as in GCM-indemiss simulation output. The total AOD from GCM-indemiss, τ^m is constrained with the ground-based observed AOD (τ^o) which is then scaled with R_{bc} to calculate the constrained BC-AOD (τ_{bc}^c) as given in equation 2.

$$\tau_{bc}^c(i,j,\overline{t}) = R_{bc}(i,j,\overline{t}) \times \tau^o(i,j,\overline{t}) \qquad (2)$$

In order to incorporate the τ_{bc}^c for calculating the RA constrained surface concentration of BC namely, SC_{bc}^{cr} a ratio (η_{bc}) between the GCM-indemiss BC concentration (SC_{bc}^m) and τ_{bc}^m is considered.

$$\eta_{bc}(i,j,\overline{t}) = \frac{SC_{bc}^m(i,j,\overline{t})}{\tau_{bc}^c(i,j,\overline{t})} \qquad (3)$$

The spatial distribution of η_{bc} is confined to the same resolution as the GCM-indemiss. Using this η_{bc} the constrained surface concentration is calculated based on the theory that the sensitivity of τ_{bc}^c to SC_{bc}^{cr} is numerically equivalent to the sensitivity of τ_{bc}^m to SC_{bc}^m.

$$SC_{bc}^{cr}(i,j,\overline{t}) = \eta_{bc}(i,j,\overline{t}) \times \tau_{bc}^c(i,j,\overline{t}) \qquad (4)$$

The constrained surface concentration of BC as obtained above by RA is evaluated with measurements.

In the PA, station height specific aerosol extinction coefficients for the corresponding grid coordinates (i, j) are taken into account. This involves the calculation of the monthly mean of the aerosol extinction coefficient (σ) vertical profile derived from Cloud Aerosol Lidar and Infrared Pathfinder Satellite Observations (CALIPSO). The extinction coefficients are available layer

5   wise at a wavelength of 532 nm and vertical resolution $dz = 0.06$ km. The previously obtained τ_{bc}^c is disaggregated vertically using the retrieved profile of the aerosol extinction coefficient (σ in km^{-1}) from CALIPSO renormalized by the CALIPSO AOD, τ^{calip} averaged during the seasonal periods (as indicated by $\bar{t}$) at given HKH LA stations to obtain the BC extinction coefficient:

$$\sigma_{bc}(i, j, z, \bar{t}) = \tau_{bc}^c(i, j, \bar{t}) \times \frac{\sigma(i, j, z, \bar{t})}{\tau^{calip}(i, j, \bar{t})} \qquad (5)$$

10   The vertical distribution of the BC concentration, termed as PA constrained concentration (SC_{bc}^{cp}), is then calculated based on the formula given below:

$$SC_{bc}^{cp}(i, j, z, \bar{t}) = \frac{\sigma_{bc}(i, j, z, \bar{t})}{\alpha_{bc}(i, j) \times dz} \qquad (6)$$

where α_{bc} is the mass extinction coefficient for BC, taken as 10–16 m^{2}g^{-1} (Ram et al., 2010). The uncertainty in the BC surface concentration from $constrsimu$ using RA, taking into account the uncertainty in observed AOD, α_{bc}, and inter-annual

15   variability in AOD, is estimated to be within 30% (Kumar et al., 2018). This using PA, through application of CALIPSO data is estimated as within 45%.

2.3   Estimation of BC concentration in snow and its impact on the annual snowmelt runoff for the glaciers under study

BC concentration in the snow (BC_c, μg kg^{-1}) during pre-monsoon and winter is calculated with the following equation:

20    $$BC_{c,(ij\bar{t})} = \frac{SC_{bc,(ij\bar{t})}^m \times v_d \times t}{\rho_{ij\bar{t}} \times d} \qquad (7)$$

where $SC_{bc,\bar{t}}^m$ is the seasonal mean for atmospheric BC mass concentration (μg m^{-3}) simulated with GCM-indemiss, v_d is the dry deposition velocity (m s^{-1}), t is the season specific time interval considered for snow deposition, $\rho_{\bar{t}}$ is the seasonal mean snow density (kg m^{-3}) and d is the snow depth (m). BC_c is calculated assuming a uniform distribution of BC in top 2 cm of pure snow, as it is more contaminated and contributes to a larger albedo reduction than the deeper layers (Tanikawa et al.,

25   2009). Deposition velocity of particles has been inferred being higher than 0.010 cm s^{-1} over land (Nho-Kim et al., 2004); the minimal v_d of 0.010 cm s^{-1} is taken in the present study (similar to Yasunari et al. (2010) for the Himalayan glacier), and a higher v_d than the above will lead to increase in estimated BC_c.

The uncertainty in the estimated BC_c is 69% due to model uncertainty in SC_{bc}^m and lack of information on v_d (model uncer-

tainty for BC dry deposition velocity is 55% consistent with that mentioned in Yasunari et al. (2013) as 0.01–0.054 cm s^{-1}).
The percentage one-sigma variability in the pre-monsoon mean of $\rho_{ij\bar{t}}$ and $SC^m_{bc,(ij\bar{t})}$ is respectively 26%–30% and 42%–55%.
This of BC_c is estimated as 50%–70%.

Deposition of atmospheric BC over the snow also takes place by wet deposition through below cloud scavenging during

5 snow fall events. Calculation of this deposition therefore requires information about size-resolved snow and BC. There is
a lack of this information for the Himalayan region from observations and therefore is estimated using numerical models
through parameterization of snow scavenging (Ming et al., 2008). Using information from Nair et al. (2013) on the rate of wet
scavenging based on atmospheric BC measurements and that on snow accumulation depth at Hanle, and snow density from
ECMWF, our estimated value of BC_c from wet deposition is 36 μg kg^{-1} for the pre-monsoon (using the prescribed snow

10 density of 195 kg m^{-3}, the value is the same as that in Nair et al. (2013)). This value is obtained in the range of 32–90 μg kg^{-1}
for the HKH glaciers extrapolating the information at Hanle for the entire HKH region and glaciers under study.

The seasonal mean of spatial distribution of snow density obtained from ECMWF is used to calculate BC_c. This calculation
is also done assuming the fixed snow density of 195 kg m^{-3} (for fresh snow) as per information from Yasunari et al. (2010) in
order to facilitate comparison between estimation of BC_c from the present study and previous studies over Himalayan stations

15 (e.g. from Nair et al. (2013)). The percentage reduction in snow albedo ($\alpha^{empirical}_{dec}$)(%) for the estimated BC concentration
in snow cover (μg kg^{-1}) is assessed using the following empirical relationship proposed by Ming et al. (2009).

$$\alpha^{empirical}_{dec} = 0.075 \times BC_{c,\bar{t}} + 0.0575 \tag{8}$$

The equation describing the relationship between BC concentration in snow and albedo reduction (Ming et al., 2009) was
obtained based on snowpack observations and model calculations. As obtained from Table 4 of Yasunari et al. (2010), the BC-

20 induced SAR over the NCOP from this equation was within -17% to 8% of that estimated for internal mixture of BC with
new snow by Hansen and Nazarenko (2004).

BC-induced SAR is also calculated from the online radiative model, Snow, Ice, and Aerosol Radiation (SNICAR) (α^{SNICAR}_{dec})
(Flanner et al., 2007) to compare with the value obtained from equation (8). This calculation is done taking the difference of
snow-albedo between two sets of simulation with SNICAR, one with BC_c and the other without BC_c. SNICAR uses param-

25 eters such as snow grain size, solar zenith angle, species concentration, albedo of the underlying ground, snowpack thickness
and snowpack density (refer to Table 3). The effective radius of snow grain size is taken as 100 μm (Warren and Wiscombe,
1980) and snowpack density and snowpack thickness is referred from ECMWF gridded archive files corresponding to the pe-
riod of present study.

The relative percentage uncertainty in estimated SAR (%) due to uncertainty in BC$_c$ is estimated as within 30%. The percent-

30 age one-sigma variability in SAR associated with the variability in $\rho_{ij\bar{t}}$ is 9%–14%. The BC-induced SAR (%) for each of
the corresponding HKH stations is calculated. When compared, it is observed that calculated SAR values from SNICAR are
lower than that using the empirical approach (refer to Figure:2(e)).

Lower values from SNICAR than empirical approach is attributed to consideration of external mixing of snow with BC,

Atmospheric
Chemistry
and Physics
Discussions

and possibly a large snow grain size (of 100 μm) for addressing snow aging; snow grain radius size of 100 μm to 1000 μm is considered for new and aged snow by Warren and Wiscombe (1980).

The consideration of old-aged snow may lead to an enhanced BC accumulation onto the snow surface and a higher reduction of snow albedo than estimated in the present study taking into account BC accumulation in the top 2 cm of pure snow (not contaminated from the pre-existing debris cover). Also, there is a possibility of enrichment of BC in snow (not taken into account in the present study) due to the predominance of sublimation compared to precipitation during the period under study, including likely a higher v_d than in the present study which justifies our assumption that we are using a lower bound estimate of SAR from what could be the actual scenario. Also, BC-induced SAR used in the sensitivity analysis of annual snowmelt runoff for a glacier (discussed in the next Section) is considered for BC_c with dry deposition only (due to lack of adequate estimation of wet deposition). All the above would thereby lead to an enhanced BC_c and impact compared to that estimated in the present study.

The present study aims to evaluate the estimated impact of BC aerosols over the glaciers in the HKH region and identify the glacial region most vulnerable to BC-induced impacts considering the lower bound estimates of their concentration in snow and the corresponding BC-induced SAR.

Table 3. Input parameters for SNICAR-Online model

Parameters	Values	reference/source
Solar zenith angle	$51.8° - 54.7°$	Oceanic and Administration
Snow grain effective radius	100 μm	Warren and Wiscombe (1980)
Snowpack thickness (m)	$\tau_{ij\bar{t}}$	ECMWF
Snowpack density ($kg\ m^{-1}$)	$\rho_{ij\bar{t}}$	ECMWF
Albedo of underlying ground	Visible: 0.2 μm	
	Near-Infrared: 0.4 μm	ECMWF
BC concentration in the snowpack (μg kg^{-1})	$BC_{cij\bar{t}}$	calculated from GCM-indemiss simulations

$\tau_{ij\bar{t}}$ = glacier wise seasonal mean value of snowpack thickness;
$\rho_{ij\bar{t}}$ = glacier wise seasonal mean value of snowpack density;
$BC_{cij\bar{t}}$ = glacier wise seasonal mean value of BC_c

2.4 Impact of BC-induced SAR on increase in annual snowmelt runoff for glacier

SAR is considered as one of the precursors of excess snow melting. To quantify the impact of BC concentration in the snowpack on annual snowmelt runoff for the glacier (also termed as annual glacier runoff in the text), we calculated the mass balance and runoff from nine selected glaciers with an energy and mass balance model for glaciers (Fujita and Ageta, 2000) (Table:1 and Figure:1(b)). As mentioned earlier, the selected glaciers are widely distributed over the HKH region and located near the zone of high BC_c values (discussed in Section 3.2). We have used a calculation scheme, in which the albedo of glacier surface was reduced from the albedo value corresponding to null value of BC_c during the control run to an albedo value of 0.5 at a given date and then runoff in the following summer season was calculated (Fujita, 2007). In the calculation, other meteorological parameters were not changed so that we evaluate the impact of surface darkening by BC only. The lower

Atmospheric
Chemistry
and Physics
Discussions

portions of the selected glaciers are covered by debris mantle. The sub-debris ice melt is highly altered with the debris thickness, and the albedo lowering by BC should not affect the ice melting under the debris layer. We, therefore, excluded the debris-covered area (Figure 1(c)), which is delineated manually by following previous studies in the eastern Himalaya (Nagai et al., 2016; Ojha et al., 2016, 2017). The calculation was performed with the ERA-Interim reanalysis data (Dee et al., 2011), but

5   precipitation was calibrated to set an initial climatic condition for each glacier, which surely affects glacier response to climate change (Sakai et al., 2015; Sakai and Fujita, 2017). The date of albedo lowering was changed at 5 day intervals for 35 years (1979–2014), and then summer mean albedo and annual runoff were calculated. The entire process is carried out for each of the glaciers. Output data set is then further analyzed statistically and discussed in Sections 3.2.1 and 3.2.2. The results of annual glacier runoff and albedo is then used to generate the data set of SAR and the corresponding annual runoff increase (ARI). The

10   BC-induced SAR values estimated for each of the glaciers under study is then interpolated with the above data set to estimate the corresponding possible range for ARI, which is analyzed in Section 3.2.1.

3   Results & discussion

3.1   Comparison between model estimated and measured BC concentration

Model estimates (free running simulations and constrained simulations as given in Table 2 and 3) are compared to measure-

15   ments. This comparison is presented as a scatter plot in Figure 2(a)–(d) for HA and LA stations. The dashed line on both the sides of the scatter plot represents a deviation factor of 2 and 0.5 respectively. A detailed performance of the model outputs with respect to the measurements is also provided in Table 4.

3.1.1   Higher altitude stations

The modeled values of simulated BC concentration from $freesimu$ at HA stations (Figure 2(a)) have more agreement to the

20   field measurements than that at LA stations (Figure 2(b)). It may be noted that HA stations are accompanied with relatively lower values (0.08 μg m^{-3} to 0.4 μg m^{-3}) of measured BC concentration compared to LA stations (1.1 μg m^{-3} to 6.5 μg m^{-3}).

   While estimates from GCM-indemiss has a normalized bias (NB) range of –6 to 30 % at HA stations for both pre-monsoon and winter seasons. Whereas those from GCM-INCA exhibits a normalized bias range of –17 to 17 % except at NCOP where

25   the overestimation by the model is as high as 2–8 times for both the seasons. SPRINTARS simulations for versions SP1 (year of simulation 2001) and SP2 (year corresponding to the year of measurement) show a general negative bias range of –21% to –70% except at Hanle where SPRINTARS exhibits a positive bias of 30% to 120%. GCM-indemiss values are hence further analyzed by comparing it with SPRINTARS (SP1 simulation). GCM-indemiss values are 3–4 times that of the SPRINTARS values for all the stations in both seasons except at Hanle where the predicted concentrations by both are similar. The variability

30   in annual mean of BC concentration (2000–2010) simulated from SPRINTARS is less than 1% and that for years corresponding to measurement is 4%–8%; this is consistent with the inter-annual variability estimated in measured BC concentration which

Atmospheric
Chemistry
and Physics
Discussions

Open Access

EGU

is 7%–9%.

The long-term SPRINTARS simulations for BC concentration are used to estimate the rate of increase (w.r.t 1961) in BC concentration and thereby in BC concentration in snow (BC_c). The predictions of the models, especially of GCM-indemiss at the high altitudes are in more sanguinity with the measured than rest other models. Discrepancies between model and

5 measurements at HA stations is likely attributed to uncertainties which stem out from instrument error, analytical errors, detection capability (pertaining to measurements of low values of atmospheric BC concentration), including degree of accuracy of model processes governing the atmospheric residence time of BC aerosols over HA stations (pertaining to $freesimu$ simulations).

3.1.2 Lower altitude Stations

10 At LA stations, estimated values of BC concentration from $freesimu$ of GCM-INCA are underestimated by a large factor, being 2 to 23 times the measured values; with that from $freesimu$ of GCM-indemiss being 2 to 11 times (refer to Table 4) and hence exhibits a better performance than that of the rest other models. At LA stations, we also evaluate the estimates from $constrsimu$ (obtained by ratio approach, RA; and profile approach, PA; refer to Section 2.2) with measurements. The comparison between model estimates ($freesimu$ and $constrsimu$) and measurements is presented as a scatter plot in Figure

15 2(b)–(c). Estimates of BC concentration from $constrsimu$ (Figure 2(c)) exhibit a better concurrence than that from $freesimu$ (Figure 2(b)) with the measured concentration at all the three LA stations. Among the $constrsimu$ (RA and PA approaches), the RA estimates deviate most of the times by a factor of two compared to the measurements (as shown by the dashed lines on both sides of the equivalent line, Figure 2(c)), amounting to about 30%–100% of the measured values, with the normalized bias being −70% to −35% except for Nainital where the pre-monsoon RA values mirror the measurements. Compared to RA, the

20 PA estimates exhibit a better coherence with the measured values, with these estimates amounting to 90-100% of measured data and a normalized bias of −14% to 13%. It is seen that the absolute bias for PA estimates is within their estimated uncertainty of as large as 45% (as discussed in Section 2.2). A better conformity of PA estimates with the measured data also emphasizes the consideration of vertical profile of BC aerosols and comparison of model values near approximate height corresponding to the field measurements. Also, a better performance of $constrsimu$ compared to $freesimu$ estimates authenticates our postulate

25 that inappropriate estimates of emission in the $freesimu$ is the primary reason for anomalous prediction by the models at LA stations which are in proximity to emission sources.

As discussed previously, $freesimu$ of GCM-indemiss has the highest conformity with the measurements at HA stations, hence we utilize BC concentration simulated in GCM-indemiss to estimate BC concentration in snow and BC-induced SAR and their impact over the HKH region.
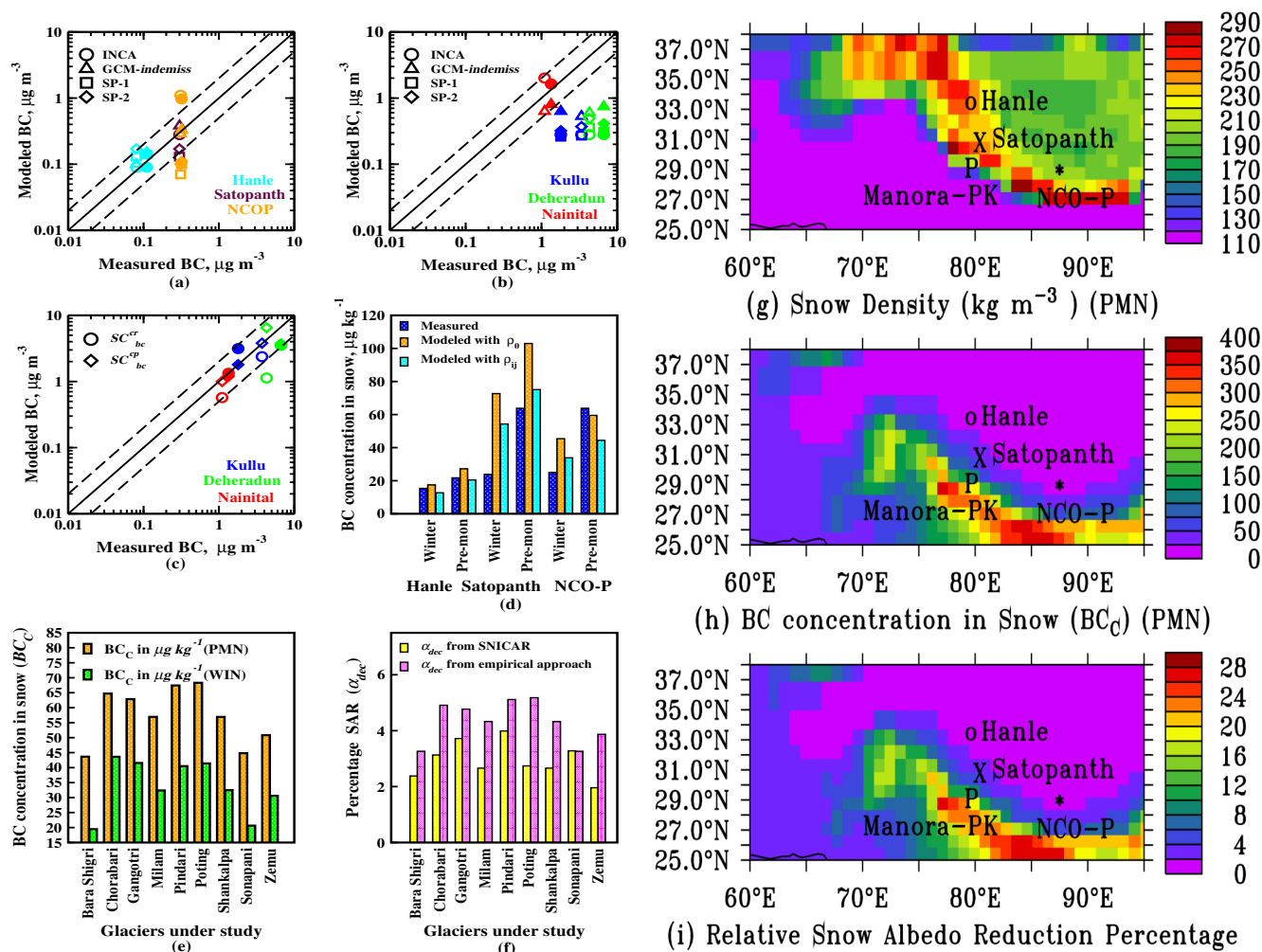
30

Figure 2. Figures showing spatio-seasonal variation of atmospheric mass BC concentration for pre-monsoon (filled symbols) and winter (unfilled symbols) for (a) Higher altitude, (b) lower altitude stations (c) Modeled versus measured atmospheric BC concentration at lower altitudes using RA and PA, (d) Station wise BC concentration in snow (BC_c) and comparison of modeled and measured values for Higher altitudes, (e) Glacier wise value of BC_c considering only dry deposition for winter and pre-monsoon season, (f) Glacier wise percentage snow albedo reduction (SAR) from both SNICAR and empirical approach for pre-monsoon; Spatial distribution of (g) averaged snow density from ECMWF for pre-monsoon season (PMN), (h) average of the modeled BC_c for PMN and (i) percentage SAR estimated using empirical approach ($\alpha_{dec}^{empirical}$) for PMN

3.2 Analysis of spatial distribution of BC concentration in snow: estimates of impact on SAR and annual glacier runoff

The comparison of BC concentration in snow (BC_c) between GCM-indemiss derived values and that obtained from available studies (e.g. Nair et al. (2013); Yasunari et al. (2010)) at HKH HA stations is presented in Figure 2(d). As mentioned earlier,

Table 4. Comparison of model output range of atmospheric BC concentration with the observed values at different stations

	HA			LA		Dehradun	Nainital
	Hanle	Satopanth	NCO-P	Kullu		Dehradun	Nainital
Model simulation							
	NMB[1] **win**[3]**(pmn**[4]**)**			**Factor**[2] **win**[3]**(pmn**[4]**)**			
GCM-INCA	17 (−17)	−7(−30)	20(3)	12(6)		23(15)	1(1)
GCM-indemiss	30(19)	27(30)	−6(3)	6(3)		11(6)	2(2)
SPRINTARS	65(30)	−58(−65)	−41(69)	12(7)		18(14)	
Constrained simulation							
				NMB[1] **win**[3]**(pmn**[4]**)**			
				Factor[2] **win**[3]**(pmn**[4]**)**			
Ratio Approach				37(55)		74(47)	48(1)
				1.6(2.2)		1.9(1.0)	3.8(1.9)
Profile Approach				−12(−1)		−4(14)	27(10)
				1.4(1.1)		0.9(0.9)	1.0(1.2)

[1] NMB: Normalized Mean Bias (%) = $\frac{Observed\ BC\ concentration\ value\ from\ literature\ -\ Modeled\ value\ of\ BC\ concentration}{Observed\ BC\ concentration\ value\ from\ literature} \times 100$

[2] Factor = $\frac{Observed\ BC\ concentration\ value\ from\ literature\ for\ LA\ stations}{Modeled\ value\ of\ BC\ concentration\ at\ respective\ stations}$

[3] win = Monthly average value of December, January and February

[4] pmn = Monthly average value of March, April and May

snow density used to estimate BC_c is extracted from the ECMWF ERA-Interim daily reanalysis data set. In order to compare our BC_c estimates with that from available study, we also estimate BC_c using the fixed snow density of 195 kg m^{-3} as done in the available studies. These estimates using fixed snow density and that using ECMWF data at HA stations are presented in Figure:2(d).

5   The estimated value of BC_c from the present study compares well with that obtained from previous work, and has a variation of 10% to 27% from the earlier studies. These estimates compare relatively well at Hanle and NCOP, however, at Satopanth during winter they are overestimated compared to the respective measured value. The percentage difference of BC_c estimates using fixed snow density with respect to that using ECMWF retrieved values is found to be 34% − 38%.

We further examine the estimates of BC_c and the relative percentage SAR (%) for the HKH glaciers under study as presented
10   in Figures 2(e) and 2(f) respectively. The pre-monsoon mean of BC_c and BC-induced SAR for the HKH glaciers is higher by 39%–76% than the winter mean. Among the glaciers, Pindari, Poting, Chorabari, and Gangotri, located over the northern HKH region near the Manora peak exhibit specifically high value of BC_c (63–68 μg kg^{-1}) and BC-induced SAR ($\approx$5%).

We also evaluate the percentage rate of increase in BC_c estimates over the HKH glaciers from 1961 to 2010 (with respect to 1961) (Figure 3(a)) estimated from the available long-term simulation of atmospheric BC concentration in SPRINTARS.
15   While there is a relative increase of BC_c from 1961 to 2010 for all glaciers under study, the percentage increase for Pindari

glacier is 26% compared to that for Zemmu, Milam and Bara Shigri which being 130%, 55% and 50% respectively.

The decadal increase indicates the possibility of the largest relative impact due to BC_c on BC-induced glacial mass balance for the Zemmu glacier (over eastern Himalayas), under conditions of similar glacier hypsometry and climatic setting. Nevertheless, the BC_c for Pindari glacier is about 7-times that for the Zemmu glacier and hence would be more vulnerable than

5 Zemmu, to these impacts. A sensitivity analysis of the change in the glacial mass balance due to relative change in hypsometry and climatic setting is discussed in Section 3.2.2.

In order to identify the location of the hot-spots over the HKH region, we also analyse the spatial distribution of pre-monsoon mean of BC_c (Figure 2(h)) and SAR (Figure 2(i)). The spatial distribution of pre-monsoon mean of snow density from the ECMWF is presented in Figure 2(g). The pre-monsoon mean of snow density is seen in the range 190–290 kg m^{-3} over the

10 HKH glaciers. Please refer to Figure 1(b) for the locations of the glaciers in the study region. High BC_c (40 μg kg^{-1} to 125 μg kg^{-1}) and the BC-induced SAR (2% to 10%) over the HKH region are located between coordinates 70°E to 90°E and 26°N to 33°N, specifically over the grids around Manora peak. A gradually increasing trend westwards from NCOP and as one moves north towards Hanle over the snow-covered (Figure 2) HKH region is observed in the spatial distribution of BC_c and SAR. The extent of the glaciers studied under this work (as listed in Figure 1(b)) over the region of 78°E to 88°E and 27°N to 34°N

15 thus allow us to locate the glaciers which are the most affected due to BC_c; this is examined in the next Section. The ablation zone of Gangotri glacier (located from the field measurements), which lies at approximately 30°93′ N and 79° E is also found to be within the zone of predicted high BC_c values. High BC_c in the range of 55 μg kg^{-1} to 100 μg kg^{-1} in the ablation zone of Gangotri near the snout, Gomukh, is estimated in the present study.

3.2.1 Estimates of impact on annual glacier runoff

20 The simulated impact of albedo reduction on annual snowmelt runoff (mm of water equivalents per year, mm w.e.y^{-1}) from glaciers using a glacial mass balance model (Fujita and Ageta, 2000) is presented in Figure 3(c). Error bars of each point is calculated as the standard deviations of the 35 years simulated period (1979-2014). Sensitivity of annual glacier runoff to albedo change (Figure 3(c)), which is the gradient of linear regression, ranges between -6834 and -9945 mm w.e.y^{-1}. This is more negative than that for a cold Tibetan glacier (about -3670 mm w.e.y^{-1}, Fujita (2007); Fujita et al. (2007)), thus implying

25 annual glacier runoff corresponding to albedo change is more sensitive (i.e. higher rate of glacier runoff increase per unit decrease in albedo) for the HKH glaciers than the Tibetan glacier. Our derived BC-induced SAR value for each of the HKH glaciers (Figure 2(f)) is then incorporated (Section 2.4) into the results of the numerical simulation to calculate the increase in annual snowmelt runoff from the glaciers which is displayed as box-plot in Figure:3(b). The Figure presents the estimated annual runoff increase (ARI) in mm w.e.y^{-1} for debris-free part of glaciers under study along with glacier wise average annual

30 recession in meters (as obtained from available observational studies, refer to Table 1). The calculated values of ARI due to BC-induced SAR (Figure:3(b)) show the median value of ARI for the HKH glaciers under study being greater than 120 mm w.e.y^{-1}, with the highest value (316 mm w.e.y^{-1}) for the Pindari glacier and followed by that for the Shunkalpa glacier (278 mm w.e.y^{-1}). Although the ARI for Milam glacier is around 261 mm w.e.y^{-1} (lower than the Pindari), this glacier witnesses the highest percentage increase (18%) of ARI w.r.t the control run (with null value of BC$_c$), followed by Pindari (16% increase).
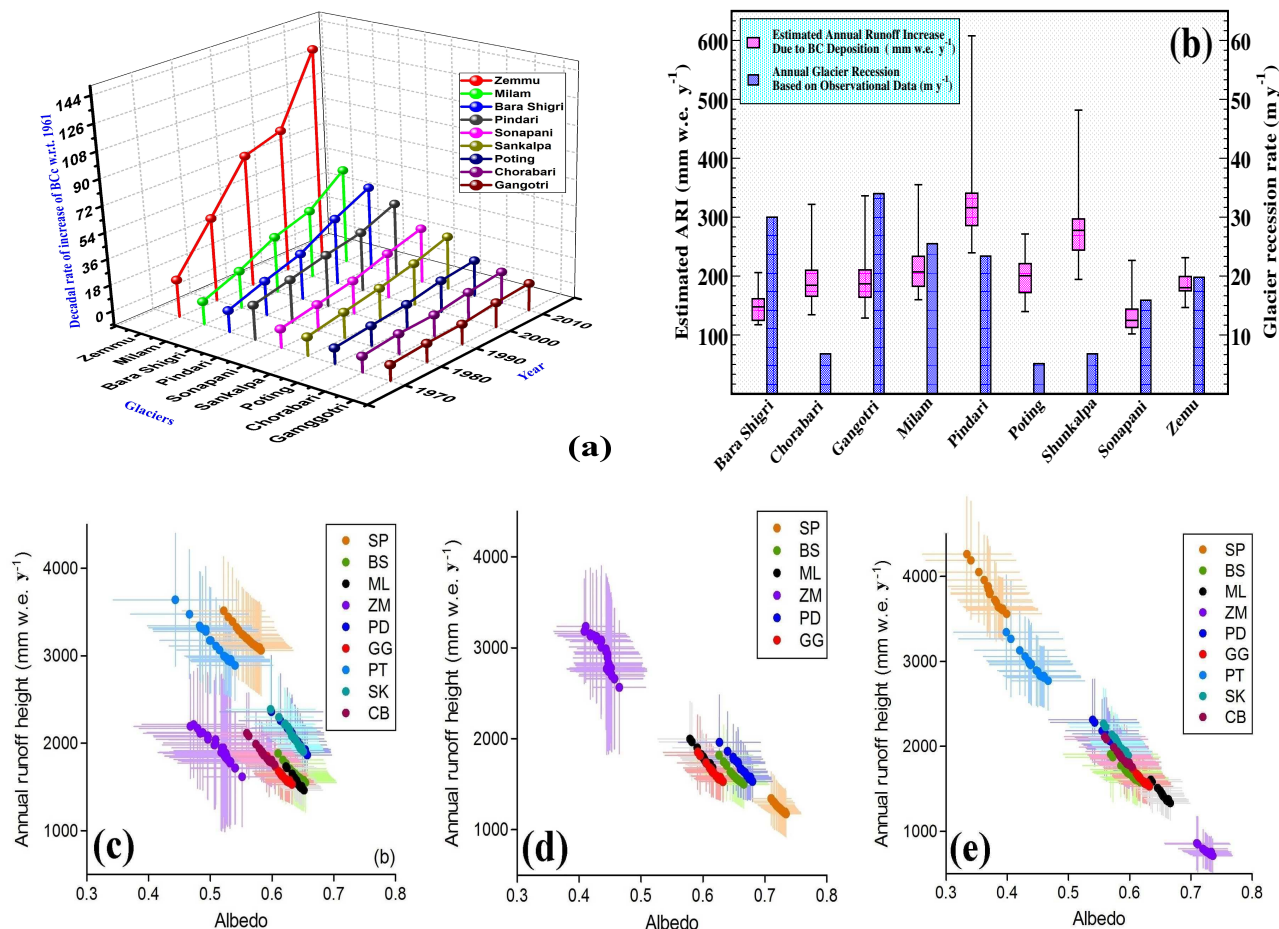
Atmospheric
Chemistry
and Physics
Discussions

Figure 3. (a) Glacier wise decadal trend (1961–2010, % rate of increase w.r.t 1961) of BC_c based on atmospheric BC concentration ($\mu g\ m^{-3}$) modeled over the glacier using SPRINTARS, (b) Estimated increase in annual glacier runoff (mm w.e.y^{-1}) and average yearly recession (m y^{-1}) for the nine glaciers, (c) Simulated impact of albedo reduction on annual glacier runoff, (d-e) Simulated impact of albedo reduction on annual glacier runoff for (d) a single glacier hypsometry at different ERA-Interim grids and (e) different glacier hypsometries at a single ERA-Interim grid

The calculated values of the rate of ARI per unit BC-induced SAR (%) as shown in Table 5, indicate this rate being specifically high (> 55 mm w.e.y^{-1} per unit % SAR) for Milam, Pindari, and Shunkalpa glacier. From the Figure, it can also be seen that the Gangotri glacier is the most rapidly shrinking one among the HKH glaciers under study, having maximum yearly recession of as high as 34 meters, (Sangewar and Kulkarni, 2011), followed by Bara Shigri, Milam, and Pindari. Five out of the total nine glaciers are retreating at a rate higher than 20 meters per year (range varying from 6.8 to 34 m y^{-1}), which is really alarming. The percentage uncertainty in albedo due to the impact of surface darkening by BC associated with the different climatic

conditions is 5%–20% and in the corresponding estimated annual snowmelt runoff is 13%–47% (Figure:3c). The uncertainty in the corresponding increase in annual snowmelt runoff (Figure:3b) is 10%–23%.

In summary, the present study leads to identify glaciers over the HKH region being vulnerable to BC-induced impacts, which includes those affected by a large value of BC_c and BC-induced SAR (e.g. Pindari, Poting, Chorabari, and Gangotri), in addition to those being specifically highly sensitive to BC-induced impacts (e.g. Shunkalpa, Pindari, Milam, and Zemmu). The Pindari glacier feeds the river Pindar which runs for 124 km with a catchment area of 1688 km before it's confluence with river Alaknanda at Karnaprayag. It is highly essential that the ARI from this glacier be quantified to manage the abundant meltwater. Our analyses show that there is an enhanced BC_c in the present decade as compared to the earlier decades due to the enhanced BC concentrations originating from anthropogenic activities.

3.2.2 Sensitivity analysis of the annual glacier runoff–albedo relationship

The estimated impact of BC_c on annual glacier runoff is affected not only by the amount of deposited BC but also by glacier hypsometry and climatic setting. To quantify these effects, we further calculated the sensitivity of annual glacier runoff to albedo change with two different configurations: (1) with a single glacier hypsometry at different ERA-Interim grids, and (2) with different glacier hypsometries at a single ERA-Interim grid. The configuration (1) demonstrates how different climatic settings affect the annual runoff sensitivity (Fig:3(d)) while configuration (2) shows how different altitudinal profiles affect the results (Fig:3(e)). We use the hypsometry of Gangotri Glacier (GG) because of its wide range in altitude (Fig:1(c)). Configuration (1) resulted in similar annual runoff heights (Fig:3(d)) and annual runoff sensitivity (GG hypsometry, Table:5) for the neighboring grids (ML and PD) except for two grids (BS and ZM). Zemmu Glacier (ZM) is located in the eastern Himalaya and thus situated higher elevation than the other glaciers (Fig:1(c)). If the GG hypsometry is applied to the ZM grid, the large ablation area should produce more meltwater under warmer condition. Albedo reduction should enhance the ice melting in such a way, warmer the condition, more will be the runoff. This is why the annual runoff sensitivity is so negative. On the other hand, Sonapani Glacier (SP) is the northwestern margin of the studies domain. Larger accumulation area of the GG glacier than the SP glacier should reduce the area-averaged annual runoff because the albedo reduction should not affect glacier melting at high altitude. Configuration (2) demonstrates how glacier hypsometry affect the amount and sensitivity of annual runoff (GG grid, Table:5 and Fig:3(e)). Neighboring glaciers (ML, PD, GG, PT, SK, and CB) show similar results to the control calculation (Fig:3(c)) while glaciers from different climate show contrasting results. The ZM glacier is situated at higher altitude than the GG glacier (Fig:1(c)), the amount and sensitivity of annual runoff are significantly reduced, and vice versa for the SP glacier (Fig:3(e) and Table:5). Spatial contrast of climate and glacier hypsometry affect how these glaciers respond to surface darkening by BC.

Table 5. Sensitivity of annual runoff and runoff increase (ARI) to albedo change for the glaciers considered in this study, along with sensitivity of annual runoff to albedo due to change in climatic condition and glacier hypsometry

Glacier Name (abbreviation)	Sensitivity of annual runoff to albedo [1] (mm w.e. y^{-1} albedo^{-1})	Sensitivity of ARI to SAR [2] (mm w.e. SAR^{-1})	Sensitivity of annual runoff to albedo for GG hypsometry [3] (mm w.e. y^{-1} albedo^{-1})	Sensitivity of annual runoff to albedo for GG grid [4] (mm w.e. y^{-1} albedo^{-1})
Bara Shigri (BS)	-6841	44.751	-7263	-6500
Chorabari (CB)	-7935	47.925	Same as GG	-7935
Gangotri (GG)	-7700	48.684	-7700	-7700
Milam (ML)	-9586	62.465	-8554	-8700
Pindari (PD)	-9031	59.341	-8198	-8093
Poting (PT)	-7971	43.041	Same as PD	-8116
Shunkalpa (SK)	-9945	64.713	Same as PD	-9357
Sonapani (SP)	-6834	39.787	-6371	-11084
Zemmu (ZM)	-7039	38.818	-12738	-5301

[1] Slope of annual runoff (mm w.e.y^{-1}) to albedo from Figure:3(c); [2] Slope of increase in annual runoff (mm w.e.) to BC induced percentage SAR; [3] Slope of annual runoff (mm w.e.y^{-1}) to albedo from Figure:3(d), where Gangotri (GG) hypsometry implies that the calculation with the same hypsometry of Gangotri Glacier (GG), as a sensitivity test of different climatic condition by using the single hypsometry; [4] Slope of annual runoff (mm w.e.y^{-1}) to albedo from Figure:3(e), where Gangotri (GG) grid implies that the calculation with the same ERA-Interim grid including Gangotri Glacier (GG), as a sensitivity test of different hypsometry by using the single ERA-Interim grid
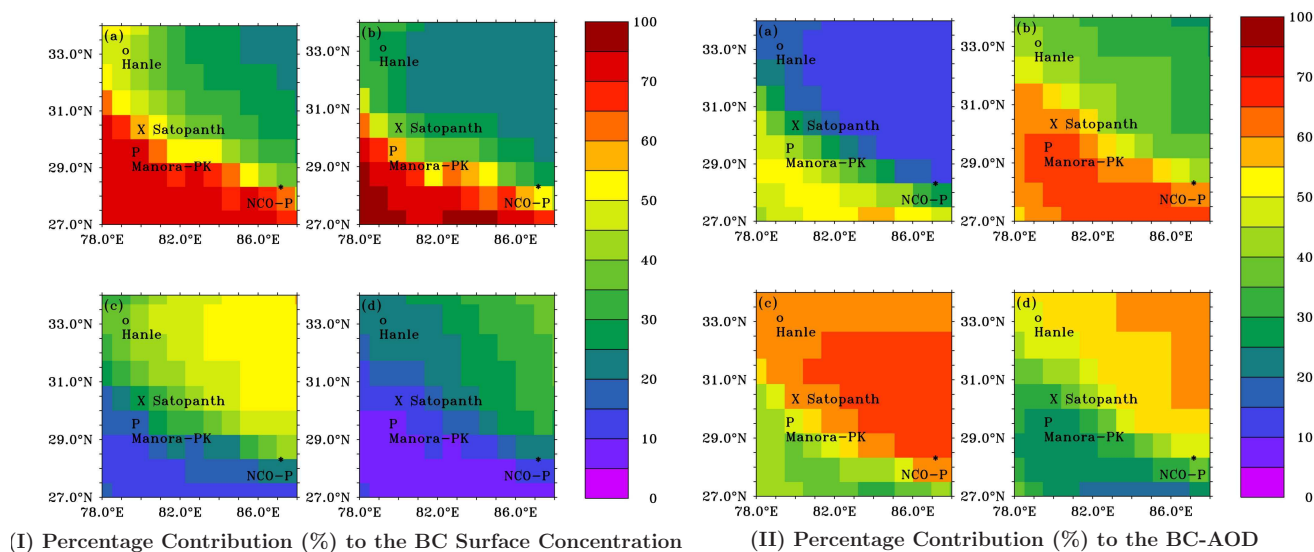

Figure 4. Spatial distribution of mean of (I) surface BC concentration and (II) BC-AOD for winter (left panel) and pre-monsoon (right panel) due to relative percentage contribution (%) of emissions from the IGP (top panels) and AFWA (bottom panels).
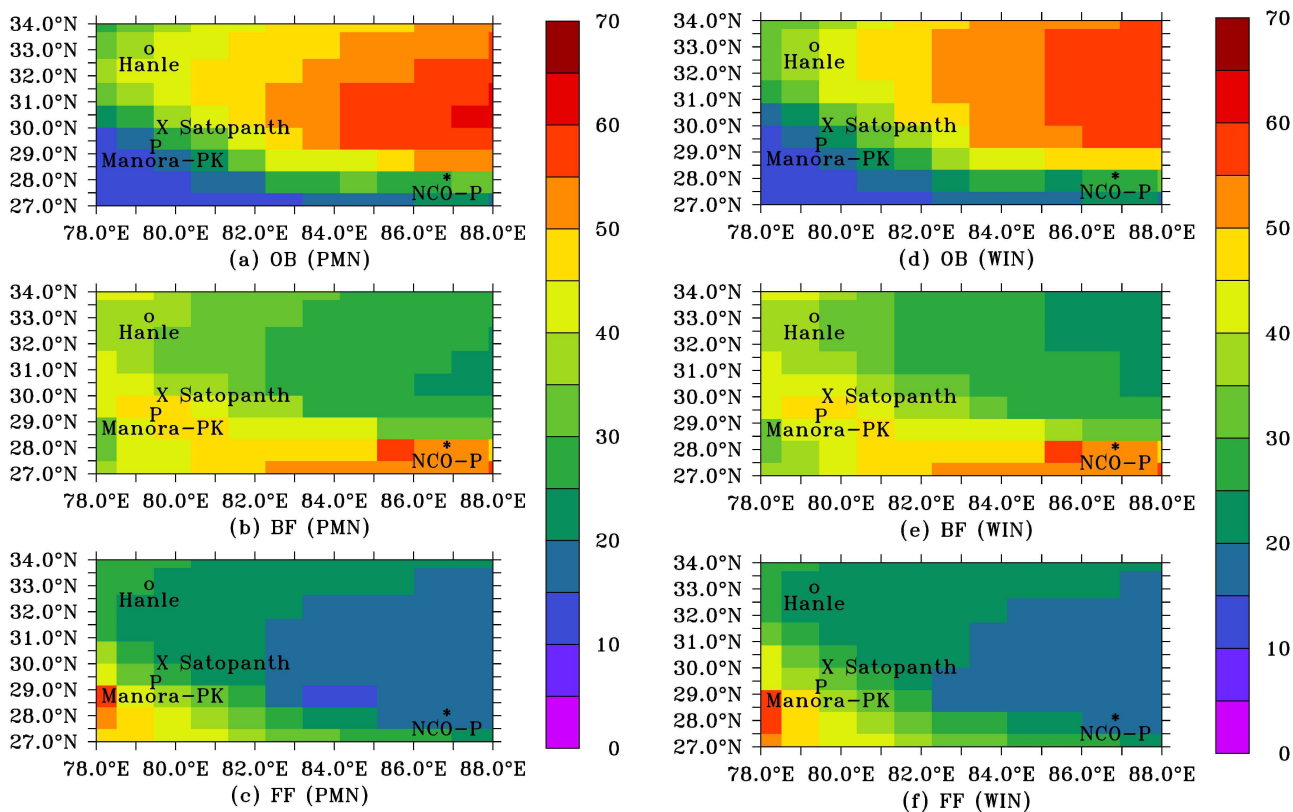
Atmospheric
Chemistry
and Physics
Discussions
Open Access
EGU

Figure 5. Spatial distribution of (left panel, a-c) pre-monsoon, and (right panel, d-f) winter mean of surface BC concentration due to relative percentage contribution (%) of BC emissions from open burning (OB), biofuel (BF) and fossil fuel (FF) combustion.

3.3 Source of origin of BC aerosols over HKH region

3.3.1 Contribution of BC emissions from near-by and far-off regions to BC aerosols

The relative distribution (%) of BC surface concentration (Figure 4(I)) and BC-AOD (Figure 4(II)) due to BC emissions originating from near-by region, IGP (BC concentration or BC-AOD due to emissions from the IGP to the total BC concentration or BC-AOD) and far-off region, Africa-west Asia (AFWA) during winter and pre-monsoon seasons over the HKH region is es-

5 timated. These estimations are done from region-tagged simulations in the GCM over the HKH region (please refer to Section 2.1). The spatial distribution (%) of winter and pre-monsoon mean of surface BC concentration (BC-AOD) due to emissions from the IGP is 70% to 90% (45% to 80%) of the total surface BC concentration (BC-AOD) over the part of the HKH region south to 30°N. This distribution decreases as we move towards the north (north to 30°N), at higher latitudes in the Himalayan

10 region. The spatial distribution (%) of surface BC concentration (BC-AOD) due to emissions from AFWA increases towards the northern grids (north to 30°N), with these being 25% to 40% (50% to 60%) in winter and 15% to 25% (40% to 55%) in pre-

Atmospheric
Chemistry
and Physics
Discussions

Open Access

EGU

monsoon. It is observed that while BC concentration and BC-AOD due to emissions from the IGP has a slightly higher value during pre-monsoon than winter, it is vice-versa for that due to emissions from AFWA. This feature is inferred likely due to emissions of biomass burning (crop-waste and forest fires) which is more prominent during pre-monsoon over the IGP but that during winter over AFWA as obtained from the information of firecounts data from satellite-based measurements (Pohl et al.,

5   2014; Verma et al., 2014). Estimates of pre-monsoon and winter mean of surface BC concentration due to relative contribution (%) of emissions from open burning (OB), biofuel (BF) and fossil fuel (FF) combustion from source-tagged (refer to Section 2.1) BC simulations in LMDZT-GCM are also presented respectively in Figures 5(a to c) and 5(d to f). These Figures indicate that while BC surface concentration during winter and pre-monsoon are influenced mostly due to biofuel emissions over part of the HKH region south to 30°N (where there is a relatively higher contribution from emissions over the IGP), these are due to

10   biomass burning over north to 30°N, thus corroborating the above inference. The high BC_c and BC-induced SAR over glaciers near to the Manora peak, over northern Himalayan region are thus found to be mainly due to contribution of BF emissions from the IGP region.

4   Conclusion

We evaluated the impact of BC aerosols and their sources of origin over the HKH region and identified the glaciers most

15   sensitive to such impacts. This is done through utilizing BC concentration estimated from the free running ($freesimu$) BC simulations with the LMDZT-GCM and SPRINTARS and that from constrained simulation ($constrsimu$) approach. Sensitivity analysis of BC-induced snow-albedo reduction (SAR) to increase in annual glacier runoff is done through numerical simulations with glacial mass balance model for identified nine glaciers.

While $freesimu$ of GCM-indemiss exhibited a relatively good comparison with available observations over the high-

20   altitude locations, the $constrsimu$ exhibited that with over the low-altitude (LA) locations. A good comparison of $constrsimu$ indicated the discrepancy in emissions in $freesimu$ being a primary reason for the anomalous performance of $freesimu$ over the LA stations. Estimates of BC concentration in snow (BC_c) was consistent with that obtained from available study, and its spatial mapping led to identify the hot-spot zone over the HKH region. Analysis of BC_c over the identified glaciers located in the vicinity of the hot-spot zone over the HKH region showed specifically high BC_c and BC-induced SAR over glaciers near

25   to the Manora peak, over northern Himalayan region (e.g., Pindari, Poting, Chorabari, and Gangotri), with their highest being that for Pindari and Poting. Using long-term BC simulations from SPRINTARS, the relative (%) rate of increase of BC_c for the present years (with respect to 1961) was the highest (130%) for the glacier (Zemmu) near eastern Himalayan region, and was five times that for the Pindari glacier; thereby indicating the largest relative impact of the BC-induced glacial mass balance for the Zemmu glacier among glaciers studied, under conditions of similar glacier hypsometry and climatic setting.

30   Sensitivity analysis of annual glacier runoff to BC-induced albedo change indicated that HKH glaciers are more sensitive than cold Tibetan glaciers. The median of annual glacier runoff increase due to BC-induced SAR was estimated to be greater than 120 mm w.e.y^{-1} for HKH glaciers with the highest being for Pindari. Among the HKH glaciers, the rate of increase in annual glacier runoff per unit BC-induced percentage SAR was specifically high for Shunkalpa, Pindari, and Milam (over

northern Himalayas). The present study provided information on specific glaciers over the HKH region as identified being vulnerable to BC-induced impacts (affected by high BC-induced SAR in addition to that being sensitive to BC-induced impacts). This information about pollution-induced impact on specific glaciers is also seen to be consistent with that on signatures of observed glacial recession indicating a relatively higher recession for Gangotri, Milam, and Pindari among the HKH glaciers.

5   While the source of BC aerosols over the HKH region south to 30°N (including the hot-spot zone) was inferred being primarily from the biofuel emissions originating in the nearby region (IGP), it was over north to 30°N from open burning emissions originating in far-off region (AFWA).

   Information on BC-induced impacts on SAR and sensitivity of annual glacier runoff over the HKH region will be utilized in a future study to understand the pollution-induced hydrological changes downstream and also to predict the fate of rivers

10   originating from the region in the long run.

5   Acknowledgments

Atmospheric
Chemistry
and Physics
Discussions

References

Babu, S. S., Chaubey, J. P., Krishna Moorthy, K., Gogoi, M. M., Kompalli, S. K., Sreekanth, V., Bagare, S., Bhatt, B. C., Gaur, V. K., Prabhu, T. P., et al.: High altitude (4520 m amsl) measurements of black carbon aerosols over western trans-Himalayas: Seasonal heterogeneity and source apportionment, Journal of Geophysical Research: Atmospheres, 116, 2011.

5 Bonasoni, P., Cristofanelli, P., Marinoni, A., Pradhan, B., Fuzzi, S., Gobbi, G., Vuillermoz, E., and Laj, P.: High concentration of black carbon observed in the high Himalayas, UNEP Black Carbon E-bulletin, 2, 15 273, 2010a.

Bonasoni, P., Laj, P., Marinoni, A., Sprenger, M., Angelini, F., Arduini, J., Bonafè, U., Calzolari, F., Colombo, T., Decesari, S., et al.: Atmospheric Brown Clouds in the Himalayas: first two years of continuous observations at the Nepal Climate Observatory-Pyramid (5079 m), Atmospheric Chemistry and Physics, 10, 7515–7531, 2010b.

10 Bonasoni, P., Cristofanelli, P., Marinoni, A., Vuillermoz, E., and Adhikary, B.: Atmospheric pollution in the Hindukush- Himalaya region: Evidence and implications for the regional climate, J. Mountain Research and Development, 32 No 4, 468–479, 2012.

Bond, T. C., Streets, D. G., Fernandes, S. D., Nelson, S. M., Yarber, K. F., Woo, J.-H., and Klimoni, Z.: A technology-based global inventory of black and organic carbon emissions from combustion, J. Geophys. Res., 109, D14203, https://doi.org/10.1029/2003JD003697, 2004.

Bond, T. C., Doherty, S. J., Fahey, D. W., Forster, P. M., Berntsen, T., DeAngelo, B. J., Flanner, M. G., Ghan, S., Karcher, B., Koch, D.,

15 Kinne, S., Kondo, Y., Quinn, P. K., Sarofim, M. C., Schultz, M. G., Schulz, M., Venkataraman, C., Zhang, H., Zhang, S., Bellouin, N., Guttikunda, S. K., Hopke, P. K., Jacobson, M. Z., Kaiser, J. W., Klimont, Z., Lohmann, U., Schwarz, J. P., Shindell, D., Storelvmo, T., Warren, S. G., and Zender, C. S.: Bounding the role of black carbon in the climate system: A scientific assesment, J. Geophys. Res., 118, 1–173, https://doi.org/10.1002/jgrd.50171, 2013.

Boucher, O. and Pham, M.: History of sulfate aerosol radiative forcings, Geophys. Res. Lett., 29, 22(1–4),

20 https://doi.org/10.1029/2001GL014048, 2002.

Cooke, W. F. and Wilson, J. J. N.: A global black carbon aerosol model, J. Geophys. Res., 101, 19,395–19,409, 1996.

Cooke, W. F., Liousse, C., Cachier, H., and Feicher, J.: Construction of a $1° \times 1°$ fossil fuel emission data set for carbonaceous aerosol and implementation and radiative impact in the ECHAM4 model, J. Geophys. Res., 104, 22,137–22,162, 1999.

Cooke, W. F., Ramaswamy, V., and Kasibhatla, P.: A general circulation model study of the global carbonaceous aerosol distribution, J.

25 Geophys. Res., 107, 4279, https://doi.org/10.1029/2001JD001274, 2002.

Dee, D. P., Uppala, S., Simmons, A., Berrisford, P., Poli, P., Kobayashi, S., Andrae, U., Balmaseda, M., Balsamo, G., Bauer, P., et al.: The ERA-Interim reanalysis: Configuration and performance of the data assimilation system, Quarterly Journal of the royal meteorological society, 137, 553–597, 2011.

Flanner, M. G., Zender, C. S., Randerson, J. T., and Rasch, P. J.: Present-day climate forcing and response from black carbon in snow, J.

30 Geophys. Res., 112, D11202, https://doi.org/10.1029/2006JD008003, 2007.

Foster, P.: Changes in Atmospheric Constituents and in Radiative Forcing, In: Climate Change 2007: The Physical Science Basis. Contribution of Working Group I to the Fourth Assessment Report of the Intergovernmental Panel on Climate Change, edited by Solomon, S., D. Qin, M. Manning, Z. Chen, M. Marquis, K.B. Averyt, M.Tignor and H.L. Miller, pp. 186-217, Cambridge University Press, 2007.

Fujita, K.: Effect of dust event timing on glacier runoff: sensitivity analysis for a Tibetan glacier, Hydrological Processes, 21, 2892–2896,

35 2007.

Fujita, K. and Ageta, Y.: Effect of summer accumulation on glacier mass balance on the Tibetan Plateau revealed by mass-balance model, Journal of Glaciology, 46, 244–252, 2000.

Fujita, K., Ohta, T., and Ageta, Y.: Characteristics and climatic sensitivities of runoff from a cold-type glacier on the Tibetan Plateau, Hydrological Processes, 21, 2882–2891, 2007.

Generoso, S., Bréon, F.-M., Balkanski, Y., Boucher, O., and Schulz, M.: Improving the seasonal cycle and interannual variations of biomass burning aerosol sources, Atmos. Chem. Phys., 3, 1211–1222, 2003.

5 Guenther, A. and et al.: A global model of natural volatile organic compound emissions, J. Geophys. Res., 91, 14,367–14,376, 1995.

Hansen, J. and Nazarenko, L.: Soot climate forcing via snow and ice albedos, Proc. Natl. Acad. sci., 101, 2, 2004.

Hourdin, F. and Armengaud, A.: The use of finite-volume methods for atmospheric advection of trace species. Part I: Test of various formulations in a general circulation model, Mon. Weather Rev., 127, 822–837, 1999.

Hourdin, F., Talagrand, O., and Idelkadi, A.: Eulerian backtracking of atmospheric tracers. II: Numerical aspects, Q. J. R. Meteorol. Soc.,
10   132, 585–603, 2006.

Jacobi, H. W., Lim, S., Menegoz, M., Ginot, P., Laj, P., and Bonasoni, P.: Black carbon in snow in the upper Himalayan Khumbu valley, Nepal, The Cryosphere, 8, 5035–5076, https://doi.org/10.5194/tcd-8-5035-2014, 2014.

Jacobson, M.: Climate response of fossil fuel and biofuel soot, accounting for soot's feedback to snow and sea ice albedo amd emmissivity, J. Geophys. Res., 109, D21201, https://doi.org/10.1029/2004JD004945, 2004.

15 Kumar, D. B., Verma, S., Boucher, O., and Wang, R.: Constrained simulation of aerosol species and sources during pre-monsoon season over the Indian subcontinent, Atmospheric Research, 214, 91–108, 2018.

Lamarque, J. F., Bond, T. C., Eyring, V., Granier, C., Heil, A., Klimont, Z., Lee, D., Liousse, C., Mieville, A., Owen, B., Schultz, M. G., Shindell, D., Smith, S. J., Stehfest, E., Aardenne, J. V., Cooper, O. R., Kainuma, M., Mahowald, N., McConnell, J. R., Naik, V., Riahi, K., and van Vuuren, D. P.: Historical (1850–2000) gridded anthropogenic and biomass burning emissions of reactive gases and aerosols:
20   methodology and application, Atmos. Chem. Phys., 10, 7017–7039, https://doi.org/10.5194/acp-10-7017-2010, 2010.

Li, Z.-X.: Ensemble atmospheric GCM simulation of climate interannual variability from 1979 to 1994, J. Climate, 12, 986–1001, 1999.

Lohmann, U. and Feichter, J.: Global indirect aerosol effects: a review, Atmospheric Chemistry and Physics, 5, 715–737, 2005.

Marinoni, A., Cristofanelli, P., Laj, P., Duchi, R., Calzolari, F., Decesari, S., Sellegri, K., Vuillermoz, E., Verza, G. P., Villani, P., and Banasoni, P.: Aerosol mass and black carbon concentrations, a two year record at NCO-P (5079m, Southern Himalayas), Atmospheric Chemistry
25   and Physics, 10, 8551–8562, https://doi.org/10.5194/acp-10-8551-2010, 2010.

Matt, F. N., Burkhart, J. F., and Pietikäinen, J. P.: Modelling hydrologic impacts of light absorbing aerosol deposition on snow at the catchment scale, Hydrology and Earth System Sciences, 22, 179, 2018.

Mehta, M., Dobhal, D., Kesarwani, K., Pratap, B., Kumar, A., and Verma, A.: Monitoring of glacier changes and response time in Chorabari Glacier, Central Himalaya, Garhwal, India, Current Science, pp. 281–289, 2014.

30 Ménégoz, M., Krinner, G., Balkanski, Y., Boucher, O., Cozic, A., Lim, S., Ginot, P., Laj, P., Gallée, H., Wagnon, P., et al.: Snow cover sensitivity to black carbon deposition in the Himalayas: from atmospheric and ice core measurements to regional climate simulations, Atmospheric Chemistry and Physics, 14, 4237–4249, 2014.

Menon, S., Koch, D., Beig, G., Sahu, S., Fasullo, J., and Orlikowski, D.: Black carbon aerosols and the third polar ice cap, Atmos. Chem. Phys., 10, 4559–4571, 2010.

35 Ming, J., , Xiao, H. C. C., Qin, D., Kang, S., Hou, S., and Xu, J.: Black carbon record based on a shallow himalayan ice core and its climate implications, Atmos. Chem. Phys., 8, 1343–1352, https://doi.org/10.5194/acp-8-1343-2008, 2008.

Ming, J., Xiao, C. D., Cachier, H., Qin, D. H., Qin, X., Li, Z. Q., and Pu, J. C.: Black carbon (bc) in the snow of glaciers in west china and its potential effects on albedos, Atmos. Research, 92, 114–123, https://doi.org/10.1016/J.ATMOSRES.2008.09.007, 2009.

Moss, R. H., Edmonds, J. A., Hibbard, K. A., Manning, M. R., Rose, S. K., Van Vuuren, D. P., Carter, T. R., Emori, S., Kainuma, M., Kram, T., et al.: The next generation of scenarios for climate change research and assessment, Nature, 463, 747–756, 2010.

Nagai, H., Fujita, K., Sakai, A., Nuimura, T., and Tadono, T.: Comparison of multiple glacier inventories with a new inventory derived from high-resolution ALOS imagery in the Bhutan Himalaya., Cryosphere, 10, 2016.

5 Nair, V. S., Babu, S. S., Moorthy, K. K., Sharma, A. K., Marinoni, A., and Ajai: Black carbon aerosols over the Himalayas: direct and surface albedo forcing, Tellus B, 65, 1019–1024, https://doi.org/10.3402/tellusb.v65i0.19738, 2013.

Naithani, A. K., Nainwal, H., Sati, K., and Prasad, C.: Geomorphological evidences of retreat of the Gangotri glacier and its characteristics, Current Science, pp. 87–94, 2001.

Nho-Kim, E.-Y., Michou, M., and Peuch, V.-H.: Parameterization of size-dependent particle dry deposition velocities for global modeling,
10   Atmospheric Environment, 38, 1933–1942, 2004.

Nuimura, T., Sakai, A., Taniguchi, K., Nagai, H., Lamsal, D., Tsutaki, S., Kozawa, A., Hoshina, Y., Takenaka, S., Omiya, S., Tsunematsu, K., Tshering, P., and Fujita, K.: The GAMDAM glacier inventory: a quality-controlled inventory of Asian glaciers, The Cryosphere, 9, 849–864, https://doi.org/10.5194/tc-9-849-2015, 2015.

Oceanic, N. and Administration, A.: NOAA Solar position calculator, http://www.esrl.noaa.gov/gmd/grad/solcalc/azel.html, 2017.

15 Ojha, S., Fujita, K., Asahi, K., Sakai, A., Lamsal, D., Nuimura, T., and Nagai, H.: Glacier area shrinkage in eastern Nepal Himalaya since 1992 using high-resolution inventories from aerial photographs and ALOS satellite images, Journal of Glaciology, 62, 512–524, 2016.

Ojha, S., Fujita, K., Sakai, A., Nagai, H., and Lamsal, D.: Topographic controls on the debris-cover extent of glaciers in the Eastern Himalayas: Regional analysis using a novel high-resolution glacier inventory, Quaternary International, 455, 82–92, 2017.

Olivier, J. G. J. and Berdowski, J. J. M., eds.: Global emissions sources and sinks, In: Berdowski, J., Guicherit, R. and B. J. Heij (Eds.), "The
20   Climate System", A. A. Balkema Publishers/Swets & Zeitlinger Publishers, Lisse, The Netherlands, ISBN: 90-5809-255-0 edn., 2001.

Painter, J. et al.: Deglaciation in the Andean region, Human development report, 2008, 2007.

Pohl, K., Cantwell, M., Herckes, P., and Lohmann, R.: Black carbon concentrations and sources in the marine boundary layer of the tropical Atlantic Ocean using four methodologies, Atmospheric Chemistry and Physics, 14, 7431–7443, 2014.

Raj, K. B. G.: Recession and reconstruction of Milam Glacier, Kumaon Himalaya, observed with satellite imagery, Current Science, pp.
25   1420–1425, 2011.

Ram, K., Sarin, M., and Tripathi, S.: Inter–comparison of thermal and optical methods for determination of atmospheric black carbon and attenuation coefficient from an urban location in northern India, Atmos. Res., 97, 335–342, https://doi.org/10.1016/j.atmosres.2010.04.006, 2010.

Ramanathan, V. and Carmichael, G.: Global and regional climate changes due to black carbon, Nat. Geosci., 1(4), 221–227, 2008.

30 Ramanathan, V., Crutzen, P., Lelieveld, J., Mitra, A., Althausen, D., Andrae, M., Cantrell, W., Cass, G., Chung, C., Clarke, A., Coakley, J., Collins, W., Conant, W., Dulac, F., Heintzenberg, J., Heymsfield, A., Holben, B., Howell, S., Hudson, J., Jayaraman, A., Kiehl, J., Krishnamurti, T., Lubin, D., McFarquhar, G., Novakov, T., Orgen, J., Prospero, I., Quinn, P., Rajeev, K., Rasch, P., Rupert, S., Sadourny, R., and Valero, F.: Indian Ocean Experiment: An integrated analysis of the climate forcing and effects of the great Indo-Asian haze, J. Geophys. Res., 106, 28,371–28,398, 2001a.

35 Ramanathan, V., Crutzen, P. J., Kiehl, J. T., and Rosenfeld, D.: Aerosols, Climate, and the Hydrological Cycle, Science, 294, 2119–2124, 2001b.

Reddy, M. S. and Venkataraman, C.: Inventory of aerosol and sulphur dioxide emissions from India: I - Fossil fuels combustion, Atmos. Environ., 36, 677–697, 2002a.

Reddy, M. S. and Venkataraman, C.: Inventory of aerosol and sulphur dioxide emissions from India: II - Biomass combustion, Atmos. Environ., 36, 699–712, 2002b.

Reddy, M. S., Boucher, O., Venkataraman, C., Verma, S., Léon, J.-F., Bellouin, N., and Pham, M.: General circulation model estimates of aerosol transport and radiative forcing during Indian Ocean Experiment, J. Geophys. Res., 109, D16205, https://doi.org/10.1029/2004JD004557, 2004.

Sakai, A. and Fujita, K.: Contrasting glacier responses to recent climate change in high-mountain Asia, Scientific reports, 7, 13 717, 2017.

Sakai, A., Nuimura, T., Fujita, K., Takenaka, S., Nagai, H., and Lamsal, D.: Climate regime of Asian glaciers revealed by GAMDAM glacier inventory, The Cryosphere, 9, 865–880, 2015.

Sangewar, C. and Kulkarni, A.: Observational studies of the recent past, Report of the Study Group on Himalayan glaciers prepared for the Office of the Principal Scientific Adviser to the Government of India, PSA/2011/2, 2576, 2011.

Schulz, M., Textor, C., Kinne, S., Balkanski, Y., Bauer, S., Berntsen, T., Berglen, T., Boucher, O., Dentener, F., Guibert, S., Isaksen, I. S. A., Iversen, T., Koch, D., Kirkevåg, A., Liu, X., Montanaro, V., Myhre, G., Penner, J. E., Pitari, G., Reddy, S., ø. Seland, Stier, P., and Takemura, T.: Radiative forcing by aerosols as derived from the AeroCom present–day and pre–industrial simulations, Atmos. Chem. Phys., 6, 5225–5246, 2006.

Spiro, P. A., Jacob, D. J., and Logan, J. A.: Global inventory of sulfur emissions with 1×1 resolution, Journal of Geophysical Research: Atmospheres, 97, 6023–6036, 1992.

Streets, D. G., Bond, T. C., Carmichael, G. R., Fernandes, S. D., Fu, Q., He, D., Klimont, Z., Nelson, S. M., Tsai, N. Y., Wang, M. Q., Woo, J.-H., and Yarber, K. F.: An inventory of gaseous and primary aerosol emissions in Asia in the year 2000, J. Geophys. Res., 108, 8809, https://doi.org/10.1029/2002JD003093, 2003a.

Takemura, T.: Distributions and climate effects of atmospheric aerosols from the preindustrial era to 2100 along Representative Concentration Pathways (RCPs) simulated using the global aerosol model SPRINTARS, Atmos. Chem. Phys., 12, 11 555–11 572, 2012.

Takemura, T., Egashira, M., Matsuzawa, K., Ichijo, H., O'ishi, R., and Abe-Ouchi, A.: A simulation of the global distribution and radiative forcing of soil dust aerosols at the Last Glacial Maximum, Atmos. Chem. Phys, 9, 3061–3073, 2009.

Takemura, T. H., Okamoto, H., Maruyama, Y., Numaguti, A., Higurashi, A., and Nakajima, T.: Global three-dimensional simulation of the aerosol optical thickness distribution of various origins, J. Geophys. Res., 105, 17,853–17,873, 2000.

Tanikawa, T., Stamnes, K., Aoki, T., Kuchiki, K., Hachikubo, A., and Sugiura, K.: Effects of snow impurities and vertical profile on snow albedo and reflectance, Eos Trans, AGU, Fall Meeting Suppl., 90, 2009.

Textor, C., Schulz, M., Guibert, S., Kinne, S., Balkanski, Y., Bauer, S., Berntsen, T., Berglen, T., Boucher, O., Chin, M., Dentener, F., Diehl, T., Easter, R., Feichter, H., Fillmore, D., Ghan, S., Ginoux, P., Gong, S., Grini, A., Hendricks, J., Horowitz, L., Huang, P., Isaksen, I., Iversen, T., Kloster, S., Koch, D., Kirkevåg, A., Kristjansson, J. E., Krol, M., Lauer, A., Lamarque, J. F., Liu, X., Montanaro, V., Myhre, G., Penner, J., Pitari, G., Reddy, S., ø. Seland, Stier, P., Takemura, T., and Tie, X.: Analysis and quantification of the diversities of aerosol life cycles within AeroCom, Atmos. Chem. Phys., 6, 1777–1813, 2006.

Verma, S., Venkataraman, C., and Boucher, O.: Origin of surface and columnar INDOEX aerosols using source- and region-tagged emissions transport in a general circulation model, J. Geophys. Res., 113, D24211, https://doi.org/10.1029/2007JD009538, 2008.

Verma, S., Venkataraman, C., and Boucher, O.: Attribution of aerosol radiative forcing over India during the winter monsoon to emissions from source categories and geographical regions, Atmos. Environ., 45, 4398–4407, https://doi.org/10.1016/j.atmosenv.2011.05.048, 2011.

Verma, S., Bhanja, S., Pani, S., and Misra, A.: Aerosol optical and physical properties during winter monsoon pollution transport in an urban environment, Environmental Science and Pollution Research, 21, 4977–4994, 2014.

Vohra, C.: Himalayan glaciers, The Himalaya: the Aspects of change, pp. 138–151, 1981.

Vohra, C. et al.: In Harnessing Eastern Himalayan Rivers, 1993.

Warren, S. G. and Wiscombe, W. J.: A model for the spectral albedo of Snow. II: Snow containing atmospheric aerosols, J. Atmos. Sci., 106, 2734–2745, 1980.

5   Yasunari, T. J., Bonasoni, P., Laj, P., Fujita, K., Vuillermoz, E., Marinoni, A., Cristofanelli, P., Duchi, R., Tartari, G., and Lau, K.-M.: Estimated impact of black carbon deposition during pre-monsoon season from Nepal Climate Observatory – Pyramid data and snow albedo changes over Himalayan glaciers, Atmos. Chem. Phys., 10, 6603–6615, https://doi.org/10.5194/acp-10-6603-2010, 2010.

Yasunari, T. J., Tan, Q., Lau, K.-M., Bonasoni, P., Marinoni, A., Laj, P., Ménégoz, M., Takemura, T., and Chin, M.: Estimated range of black carbon dry deposition and the related snow albedo reduction over Himalayan glaciers during dry pre-monsoon periods, Atmospheric
10   environment, 78, 259–267, 2013.